High-quality factor Ta_2O_5-on-insulator resonators with ultimate thermal stability

J. RASMUS BANKWITZ[1,2,3,4], MARTIN A. WOLFF[1,2,3], ADRIAN S. ABAZI[1,2,3], PIERRE-MAURICE PIEL[1], LIN JIN[1,2,3], WOLFRAM H. P. PERNICE[2,3,4], URSULA WURSTBAUER[1,3], AND CARSTEN SCHUCK[1,2,3,*]

[1] *Institute of Physics, University of Münster, Wilhelm-Klemm-Str. 10, 48149 Münster, Germany*
[2] *Center for Nanotechnology (CeNTech), Heisenbergstr. 11, 48149 Münster, Germany*
[3] *Center for Soft Nanoscience (SoN), Busso-Peus.Str. 10, 48149 Münster, Germany*
[4] *Kirchhoff-Institute for Physics, Heidelberg University, Im Neuenheimer Feld 227, 69120 Heidelberg, Germany*
[*] *carsten.schuck@uni-muenster.de*

Compiled July 3, 2023

Experiments in photonics, laser optics and quantum technology require low loss, thermal and mechanical stability. While photonic integrated circuits on monolithic chips achieve interferometric stability, important nanophotonic material systems suffer from propagation loss, thermal drift and noise that prevent, for example, precise frequency stabilization of resonators. Here we show that tantalum pentoxide (Ta_2O_5) on insulator micro-ring resonators combine quality factors beyond 1.8 Mio. with vanishing temperature-dependent wavelength shift in the relevant 70 K to 90 K temperature range. Our Ta_2O_5-on-SiO_2 devices will thus enable athermal operation at liquid nitrogen temperatures, paving the way for ultra-stable low-cost resonators, as desired for wavelength division multiplexing, on chip frequency stabilization and low noise optical frequency comb generation.

http://dx.doi.org/10.1364/ao.XX.XXXXXX

Performing experiments in ultra-low noise environments has become a crucial requirement in many branches of optics. State-of-the-art optical clocks, precision spectroscopy, nonlinear optics, and quantum technology implementations are extremely sensitive to both mechanical noise as well as thermal noise processes. This is exemplified by the enormous challenges involved in laser frequency stabilization with ultra-high quality factor (Q) Fabry-Perot cavities fabricated from ultra-low expansion glasses or even single crystal materials [1–3]. Photonic integrated circuits (PICs) allow for overcoming mechanical stability issues by fabricating resonators out of dielectric thin film systems on monolithic chips. While low cost and small device footprints due to strong mode confinement in high refractive index dielectrics constitute some advantages over bulk optic implementations, most PIC resonators suffer from noise introduced by variations in humidity, pressure, and, most importantly, temperature [4, 5]. The corresponding thermo-refractive noise of a PIC resonator is directly dependent on the thermo-optic and thermal expansion coefficients of the respective nanophotonic material system [6]. To realize stable micro-resonators with high quality factors a PIC platform further needs to achieve ultra-low optical loss.

Here we show that Tantalum Pentoxide-on-insulator (Ta_2O_5) PICs can satisfy these challenging demands when cooled to liquid nitrogen temperatures. Ta_2O_5 is emerging as a CMOS compatible nanophotonic material platform with optical properties that uniquely benefit a broad range of applications in metrology, nonlinear optics and quantum technologies [7–11]. Importantly, Ta_2O_5 offers high refractive index contrast to SiO_2, resulting in stable nanophotonic devices with compact footprints due to strong mode confinement [12–14]. Ta_2O_5 further features a wide transparency window from the ultraviolet to the infrared (0.28 µm-8 µm) [15], extremely low levels of intrinsic material fluorescence under optical excitation [16], negligible two photon absorption [17], and a relatively large third order optical nonlinearity. These features have allowed quantum emitter integration into Ta_2O_5 waveguides and the demonstration of nonlinear optical effects such as super continuum generation and spontaneous four wave mixing [18–21]. However, all applications to date have focused on room temperature operation, where thermo-refractive noise in Ta_2O_5-on-SiO_2 is comparable to other established nanophotonic platforms. Here, we investigate Ta_2O_5 on insulator micro-ring resonators over a large temperature range, extending the device operation down to 3 K. At liquid nitrogen temperatures we find minimal Temperature Dependent Wavelength Shift (TDWS) for wavelengths in the telecommunication C-band, thus giving rise to a new class of temperature stable high quality-factor devices with relaxed cooling requirements.

We assess the thermal stability of Ta_2O_5 PICs by extracting the TDWS of high-quality factor micro-ring resonances, which are cooled from room temperature to 3 K in a closed cycle cryostat. We employ spectroscopic ellipsometry (SE) of the Ta_2O_5-on-SiO_2 sample over a similar temperature range to determine the thermal expansion coefficient and then extract the thermo-optic coefficient from the TDWS measurements. This technique allows for separating the contributions of (Ta_2O_5) waveguide and (SiO_2) substrate on the thermal behavior of the device.

To best assess the intrinsic properties of Ta_2O_5 devices, we design micro-ring resonators for multi-mode operation, featuring wider waveguides in which fundamental propagation modes

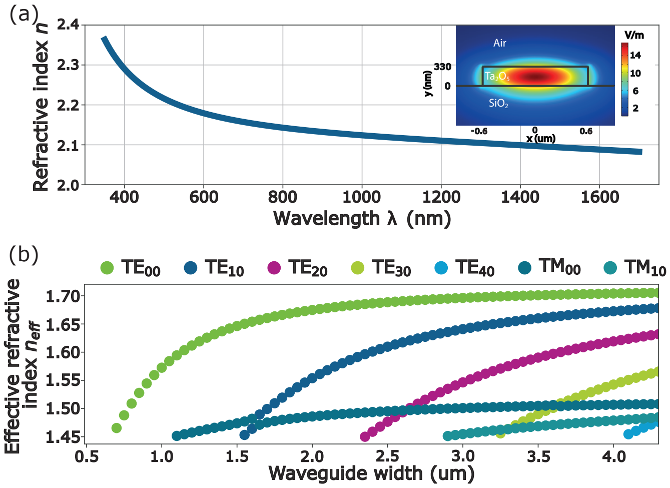

Fig. 1. (a) Refractive index of a Ta_2O_5 thin film, determined via multilayer modeling of spectroscopic ellipsometry. (inset) Simulated optical mode profile in a Ta_2O_5 ridge waveguide (b) FEM simulations of effective refractive indices for propagating modes in Ta_2O_5 waveguides of different width.

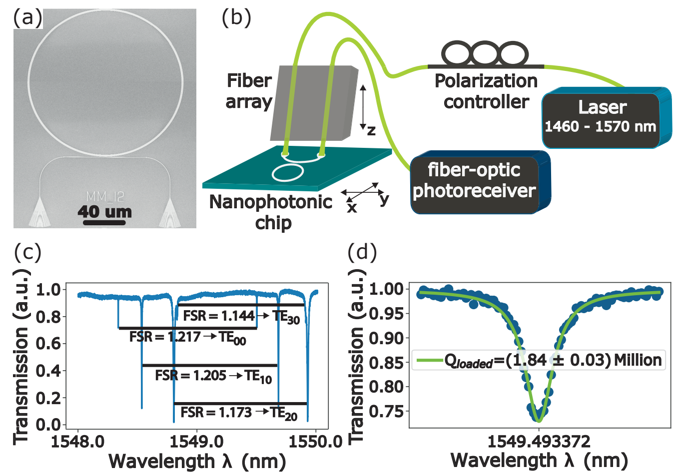

Fig. 2. (a) Scanning electron micrograph of a Ta_2O_5-on-insulator ring resonator. (b) Setup for quality factor measurements and detection of the TDWS (c) Resonance spectrum of a ring resonator and corresponding resonator modes as extracted from the FSR. (d) Single resonance of a multimode waveguide with a loaded quality factor of approx. 1.8 Mio. The quality factor is obtained from fitting a Lorentzian line shape to the data.

are less affected by scattering at waveguide sidewalls, leading to higher quality factors. We first record variable angle spectroscopic ellipsometer (VASE) data over a large wavelength range from 350 nm – 1800 nm at room temperature (Woolam M-2000) and fit a multilayer model to the ellipsometric spectra via regression analysis [22]. This procedure allows for extracting optical parameters such as refractive index n(λ), extinction coefficient $\kappa(\lambda)$ and film thickness for each layer, which constitute essential input for nanophotonic device design. The resulting n(λ) of the Ta_2O_5 film with a nominal thickness of 330 nm is shown in Figure 1 a. From electromagnetic field simulations using the finite element method (FEM, Comsol Multiphysics), we find that Ta_2O_5 waveguides of 330 nm × 1.2 µm cross section on SiO_2 substrates predominantly support the fundamental transverse electric (TE00) mode at 1550 nm wavelength, as shown in the inset of Figure 1 a, which we use as single-mode feed waveguides. Multimode operation up to TE40, on the other hand, is possible in waveguides of 4 µm width, as shown in Figure 1 b, which we chose for the micro-ring resonators. To minimize bending loss, we chose to work with a micro-ring diameter of 150 µm.

We fabricate the micro-ring resonator devices, as shown in Figure 2 a, from 330 nm ion beam sputter deposited Ta_2O_5 thin films on a 3.3 µm buried oxide layer on a silicon handle wafer (thicknesses are nominal values). Grating couplers, waveguides and micro-ring resonators are patterned via electron beam lithography using a negative tone photoresist (ma-N 2403, micro resist technology) and reactive ion etching in CF_4-CHF_3-Ar chemistry. Each sample is annealed in oxygen enriched N_2 atmosphere at 600 °C for 6 h, which was found to notably reduce propagation loss of ion-beam sputtered Ta_2O_5 thin films [23–25], as can be inferred from determining the Q-factors of micro-ring resonators as a function of annealing temperature .

We characterize the resonator devices in transmission measurements with a sweep-laser in the telecom C-band (Toptica CTL-1500), as shown in Figure 2 b. For measurements in the 300 K to 3 K temperature range the chip is mounted inside a closed cycle cryostat (ICEOxford Dry ICE 1K) on a cryogenic 3-axes translation stage (Attocube ANPxyz101). The setup allows for positioning the grating couplers of a device under test under an optical fiber array, which also collects transmitted light for intensity measurements with a photodiode (NewFocus 2053-FC-M). The recorded spectra (see Figure 2 c) allow for identifying the modes guided inside the resonator by comparing experimentally observed free spectral ranges (FSR) with simulation results. For the TE00 mode we find loaded quality factors up to $Q = 1.84$ Mio. from fitting a Lorentzian function to the data acquired with slightly over-coupled devices at room temperature, as shown in Figure 2 d.

The TDWS, given as [26]

$$\Delta\lambda \sim \frac{n_{\mathrm{eff}}\alpha}{n_{\mathrm{eff,g}}}\lambda\Delta T \quad \textbf{(1)}$$

describes fluctuation of the resonance wavelength λ of the micro-ring in terms of device temperature and the coefficient of thermal expansion (CTE) α that follows a $\frac{1}{L} \times \left(\frac{\delta L}{\delta T}\right)$ dependence on optical path length L inside the resonator. Here it is noteworthy that the optical mode extends from the Ta_2O_5 waveguide into the SiO_2 substrate (see Figure 1 a inset) and both material components contribute to the TDWS. We experimentally determine the TDWS $\Delta\lambda$ by following the center wavelength of a single high Q-factor resonance when cooling the chip from room temperature to 3 K.

The data in Figure 3 a shows the resonance wavelength as determined from a Lorentzian fit to the transmitted power data for a large number of temperature values, measured at the backside of the sample. The TDWS is here expressed relative to the resonance wavelength at 3 K. Notably the gradient of the TDWS vanishes not only for temperatures < 15 K, where several quantum technology devices are being operated, but also in the 70 K – 90 K temperature range, which can conveniently be reached with economic liquid nitrogen (LN) cooling. In these temperature regions Ta_2O_5-on-SiO_2 devices achieve ultimate thermal stability.

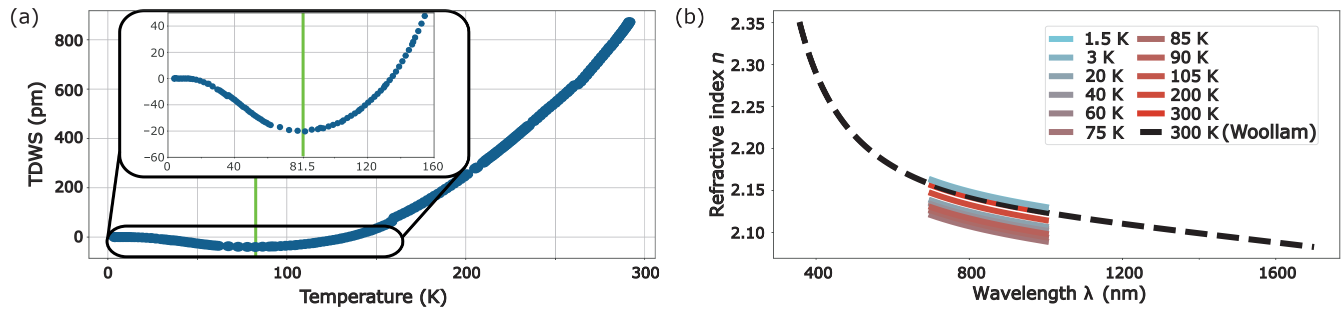

Fig. 3. (a) TDWS vs temperature. The measured resonance wavelength at 3 K serves as a reference for the TDWS at other temperatures. The inset shows a zoom in to temperature range around 80 K where the TDWS-gradient changes sign. (b) Refractive index of a Ta_2O_5 thin film for different temperatures determined from SE measurements (Accurion ellipsometer) from 1.5 K to room temperature. The data measured with the Woollam ellipsometer (same as Figure 1 a) is plotted to show the close agreement of the results from two different Ellipsometers accessing different wavelength ranges.

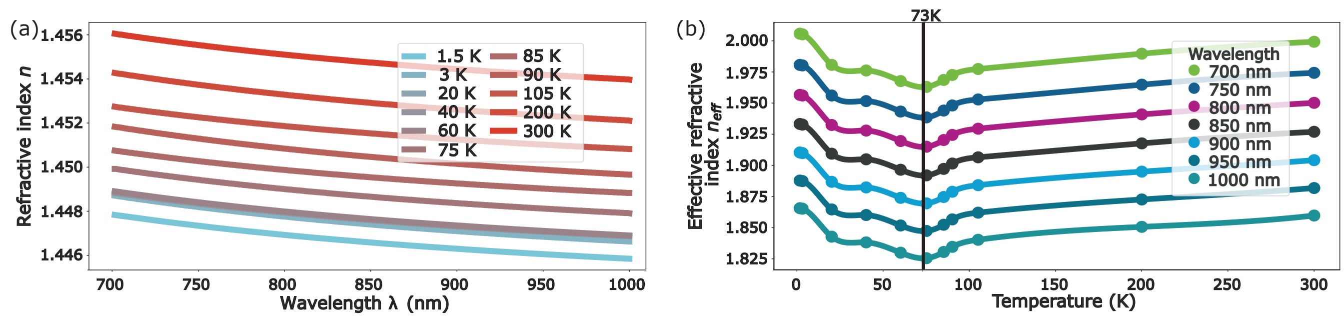

Fig. 4. ((a) Refractive index of the SiO_2 substrate for different temperatures, measured from 1.5 K to room temperature with the Accurion SE. The data for SiO_2 and Ta_2O_5 are determined from the same ellipsometer measurement, thus enabling effective refractive index simulations. (b) Effective refractive index simulated via FEM for 1.2 µm wide, 330 nm thick Ta_2O_5-on-SiO_2 waveguides.

To investigate the origin of this behavior, we combine the aforementioned room temperature SE measurements over large spectral bandwidth (see Figure 1 a) with temperature dependent SE measurements performed with a customized Accurion EP4 spectroscopic imaging ellipsometer, covering the 450 nm – 1000 nm spectral range. The ellipsometer is combined with a closed cycle cryostat with an adiabatic demagnetization refrigerating (ADR) stage (Kiutra S-Type Optical) with a special designed, home-built cold-finger and vacuum can. The vacuum can and radiation shields are equipped with windows for direct optical access. The angle of incidence used in the temperature dependent SE measurements was fixed to 50 ° and is adjusted to the window configuration of the cryostat in order to ensure orthogonal light beams through the windows to avoid their impact on SE measurements while maintaining suitable reflectance contrast between s- and p- polarized light.

The refractive indices n(λ) for the thin films are again determined from fits to the measured SE spectra using the same multilayer model as for spectrally extended room temperature Woollam SE measurements. To model the SiO_2 film a Sellmeier term, as an improvement of the classical Cauchy function, was used and for the Ta_2O_5 film a combination of a Tauc-Lorentz term, a UV-pole and an Eps-fix term was employed [27]. The Tauc-Lorentz term is a refinement of the Lorentz oscillator model describing the lowest direct interband transition. The UV-pole represents a pole in the real part of the dielectric function describing higher lying interband transitions far from the experimental accessible energy range still influencing the linear light-matter interaction in the measured wavelength range. The Eps-fix term establishes the light dispersion in the high-energy limit with ϵ_∞. The wavelength resolved refractive indices n(λ) for Ta_2O_5 and SiO_2 thin films for the temperature range from 1.5 K to room temperature are shown in Figure 3 b and Figure 4 a, respectively. The extracted film thicknesses from fits to the model with typical root mean squared error (RMSE) values of 8 from regression analysis are rather constant in the investigated temperature range and yield 3.49 µm for SiO_2 and 318 nm for Ta_2O_5, respectively, which is within the fabrication tolerances of the nominal thickness values .

Extrapolation of the temperature dependent data into the telecom C-band, where no low-temperature compatible ellipsometry capabilities were available to us, is accompanied by increasing uncertainties. We however recognize that the dispersion function is flat in this wavelength regime and no wavelength-dependent variations of the relative differences in the temperature dependencies of the refractive index n_λ(T) for fixed wavelengths λ occur in the experimentally utilized wavelength range from 700 nm to 1000 nm, as seen in Figure 3 b. We further find that FEM simulations, similar to those shown in Figure 1, but based on low-temperature ellipsometry data, yield effective refractive indices for our nanophotonic devices that show vanishing gradients in a temperature range that coincides with the findings in TDWS measurements (see Figure 4 b). For these FEM simulations we neglect the CTE, which accounts for strain of all materials in the layer stack. Such treatment is adequate because the 525 µm thick silicon substrate contributes by far the largest material portion as compared to the 3.3 µm SiO_2 and 330 nm Ta_2O_5 thin films [28]. We note that the CTE of the silicon substrate is on the order of $1 \times 10^{-6}\,\mathrm{K}^{-1}$ [29, 30], leading to a variation of a few nanometers over the 300 K temperature range, which has negligible influence on the effective refractive index of a nanophotonic device. In addition, SiO_2 and Ta_2O_5 are rather soft amorphous films and hence much less prone to strain caused by lattice mismatch.

On the other hand, the CTE has a noticeable effect on the coupling conditions and the free spectral range of the resonator even for small changes of the microring radius. Consequently, the thermal expansion coefficient α contributes considerably to the TDWS depicted in Figure 3 a. The corresponding functional behavior of the TDWS (see also Figure 4 b) resembles that of the slope of the expansion of silicon with a minimum at 85 K [29, 30]. From Equation 1 we conclude that the product of the CTE and the effective refractive index results in a shift of the global minimum in agreement with our measured TDWS. With effective refractive index and CTE reaching minimal values at 73 K and 85 K, respectively, we find optimal thermal device stability at 81.5 K. Realizations of thermally stable devices, such as the resonators considered here, will further benefit from slow variations of CTE, effective refractive index and TDWS around their respective minimal values, thus providing stable operation over an extended temperature range.

In summary, we show that Ta_2O_5-on-insulator photonic integrated circuits allow for combining low-loss waveguiding with ultimate thermal stability. Optimal thermal conditions are found at 81.5 K by investigating the TDWS of a cryogenically cooled micro-ring resonator with loaded quality factors in excess of 1.8 Mio. Spectroscopic ellipsometry under cryogenic conditions provides evidence for the contributions of the temperature-dependent effective refractive index and CTE to the TWDS. Our results establish the Ta_2O_5-on-insulator nanophotonic platform as an ideal choice for a wide range of applications requiring ultimate thermal stability, which is straightforwardly achievable at cost-efficient liquid nitrogen temperatures.

Funding. Ministerium für Kultur und Wissenschaft des Landes Nordrhein-Westfalen (421-8.03.03.02–130428). German Science Foundation (DFG) via grant WU 637/7-1.

Acknowledgments. We would like to thank the Münster Nanofabrication Facility (MNF) for their support in nanofabrication related matters. C.S. acknowledges support from the Ministry for Culture and Science of North Rhine-Westphalia (421-8.03.03.02–130428). U.W. acknowledge support from the German Science Foundation (DFG) for financial support via grant WU 637/7-1.

Disclosures. The authors declare no conflicts of interest.

Data Availability Statement. Data underlying the results presented in this paper are not publicly available at this time but may be obtained from the authors upon reasonable request.

REFERENCES

1. A. Didier, J. Millo, B. Marechal, C. Rocher, E. Rubiola, R. Lecomte, M. Ouisse, J. Delporte, C. Lacroûte, and Y. Kersalé, Appl. Opt. **57**, 6470 (2018).
2. J. M. Robinson, E. Oelker, W. R. Milner, W. Zhang, T. Legero, D. G. Matei, F. Riehle, U. Sterr, and J. Ye, Optica **6**, 240 (2019).
3. A. W. Elshaari, I. E. Zadeh, K. D. Jons, and V. Zwiller, IEEE Photonics J. **8**, 1 (2016).
4. S. Kyatam, D. Mukherjee, H. Neto, and J. C. Mendes, Appl. Opt. **58**, 6126 (2019).
5. J. Punch, "Thermal challenges in Photonic Integrated Circuits," in *2012 13th International Thermal, Mechanical and Multi-Physics Simulation and Experiments in Microelectronics and Microsystems,* (IEEE, 2012), pp. 6–6.
6. Q. Zhao, R. O. Behunin, P. T. Rakich, N. Chauhan, A. Isichenko, J. Wang, C. Hoyt, C. Fertig, M. h. Lin, and D. J. Blumenthal, APL Photonics **5**, 116103 (2020).
7. G. Moody, V. Sorger, P. Juodawlkis, W. Loh, C. Sorace-Agaskar, A. E. Jones, K. Balram, J. Matthews, A. Laing, M. Davanco, L. Chang, J. Bowers, N. Quack, C. Galland, I. Aharonovich, M. Wolff, C. Schuck, N. Sinclair, M. Loncar, T. Komljenovic, D. M. Weld, S. Mookherjea, S. Buckley, M. Radulaski, S. Reitzenstein, G. S. Agarwal, B. Pingault, B. Machielse, D. Mukhopadhyay, A. V. Akimov, A. Zheltikov, K. Srinivasan, W. Jiang, T. McKenna, J. Lu, H. Tang, A. H. Safavi-Naeini, S. Steinhauer, A. Elshaari, V. Zwiller, P. Davids, N. Martinez, M. Gehl, J. Chiaverini, K. Mehta, J. Romero, N. Lingaraju, A. M. Weiner, D. Peace, R. Cernansky, M. Lobino, E. Diamanti, R. Camacho, and L. Trigo Vidarte, J. Physics: Photonics (2021).
8. C. Chaneliere, J. Autran, R. Devine, and B. Balland, Mater. Sci. Eng. R: Reports **22**, 269 (1998).
9. S. Ezhilvalavan and T. Y. Tseng, J. Mater. Sci. Mater. Electron. **10**, 9 (1999).
10. L. Splitthoff, M. A. Wolff, T. Grottke, and C. Schuck, Opt. Express **28**, 11921 (2020).
11. M. A. Wolff, S. Vogel, L. Splitthoff, and C. Schuck, Sci. Reports **10**, 17170 (2020).
12. L. Gao, F. Lemarchand, and M. Lequime, Opt. express **20**, 15751 (2012).
13. H. H. Li, J. Phys. Chem. Ref. Data **9**, 658 (1980).
14. I. H. Malitson, Josa **55**, 1209 (1965).
15. J. A. Black, R. Streater, K. F. Lamee, D. R. Carlson, S.-P. Yu, and S. B. Papp, Opt. Lett. **46**, 820 (2021).
16. P. P. J. Schrinner, J. Olthaus, D. E. Reiter, and C. Schuck, arXiv preprint arXiv:2011.11111 (2020).
17. M. Belt, M. L. Davenport, J. E. Bowers, and D. J. Blumenthal, Optica **4**, 536 (2017).
18. A. Eich, T. C. Spiekermann, H. Gehring, L. Sommer, J. R. Bankwitz, P. P. J. Schrinner, J. A. Preuß, S. M. de Vasconcellos, R. Bratschitsch, W. H. P. Pernice, and others, arXiv preprint arXiv:2104.11830 (2021).
19. Y. Zhao, M. Jenkins, P. Measor, K. Leake, S. Liu, H. Schmidt, and A. R. Hawkins, Appl. Phys. Lett. **98**, 091104 (2011).
20. T. Kaji, T. Yamada, R. Ueda, X. Xu, and A. Otomo, Opt. Express **19**, 1422 (2011).
21. M. Timmerkamp, N. M. Lüpken, S. A. Abazi, J. R. Bankwitz, C. Schuck, and C. Fallnich, arXiv preprint arXiv:2306.05073 (2023).
22. K. Nisi, S. Subramanian, W. He, K. A. Ulman, H. El-Sherif, F. Sigger, M. Lassaunière, M. T. Wetherington, N. Briggs, J. Gray, A. W. Holleitner, N. Bassim, S. Y. Quek, J. A. Robinson, and U. Wurstbauer, Adv. Funct. Mater. **31**, 2005977 (2021).
23. H. Demiryont, J. R. Sites, and K. Geib, Appl. Opt. **24**, 490 (1985).
24. R. Ramprasad, J. Appl. Phys. **94**, 5609 (2003).
25. H. Jung, S.-P. Yu, D. R. Carlson, T. E. Drake, T. C. Briles, and S. B. Papp, Optica **8**, 811 (2021).
26. H. Xu, M. Hafezi, J. Fan, J. M. Taylor, G. F. Strouse, and Z. Ahmed, Opt. Express **22**, 3098 (2014).
27. H. Fujiwara, *Spectroscopic Ellipsometry* (Wiley, 2007).
28. K. Johnson, N. Alshamrani, D. Almutairi, A. Grieco, C. Horvath, J. N. Westwood-Bachman, A. McKinlay, and Y. Fainman, Opt. Express **30**, 46134 (2022).
29. J. Rodriguez, S. A. Chandorkar, G. M. Glaze, D. D. Gerrard, Y. Chen, D. B. Heinz, I. B. Flader, and T. W. Kenny, J. Microelectromechanical Syst. **27**, 800 (2018).
30. K. G. Lyon, G. L. Salinger, C. A. Swenson, and G. K. White, J. Appl. Phys. **48**, 868 (1977).

FULL REFERENCES

1. A. Didier, J. Millo, B. Marechal, C. Rocher, E. Rubiola, R. Lecomte, M. Ouisse, J. Delporte, C. Lacroûte, and Y. Kersalé, “Ultracompact reference ultralow expansion glass cavity,” Appl. Opt. **57**, 6470 (2018).
2. J. M. Robinson, E. Oelker, W. R. Milner, W. Zhang, T. Legero, D. G. Matei, F. Riehle, U. Sterr, and J. Ye, “Crystalline optical cavity at 4 K with thermal-noise-limited instability and ultralow drift,” Optica **6**, 240 (2019).
3. A. W. Elshaari, I. E. Zadeh, K. D. Jons, and V. Zwiller, “Thermo-Optic Characterization of Silicon Nitride Resonators for Cryogenic Photonic Circuits,” IEEE Photonics J. **8**, 1–9 (2016).
4. S. Kyatam, D. Mukherjee, H. Neto, and J. C. Mendes, “Thermal management of photonic integrated circuits: impact of holder material and epoxies,” Appl. Opt. **58**, 6126 (2019).
5. J. Punch, “Thermal challenges in Photonic Integrated Circuits,” in *2012 13th International Thermal, Mechanical and Multi-Physics Simulation and Experiments in Microelectronics and Microsystems,* (IEEE, 2012), pp. 6–6.
6. Q. Zhao, R. O. Behunin, P. T. Rakich, N. Chauhan, A. Isichenko, J. Wang, C. Hoyt, C. Fertig, M. h. Lin, and D. J. Blumenthal, “Low-loss low thermo-optic coefficient Ta2O5 on crystal quartz planar optical waveguides,” APL Photonics **5**, 116103 (2020).
7. G. Moody, V. Sorger, P. Juodawlkis, W. Loh, C. Sorace-Agaskar, A. E. Jones, K. Balram, J. Matthews, A. Laing, M. Davanco, L. Chang, J. Bowers, N. Quack, C. Galland, I. Aharonovich, M. Wolff, C. Schuck, N. Sinclair, M. Loncar, T. Komljenovic, D. M. Weld, S. Mookherjea, S. Buckley, M. Radulaski, S. Reitzenstein, G. S. Agarwal, B. Pingault, B. Machielse, D. Mukhopadhyay, A. V. Akimov, A. Zheltikov, K. Srinivasan, W. Jiang, T. McKenna, J. Lu, H. Tang, A. H. Safavi-Naeini, S. Steinhauer, A. Elshaari, V. Zwiller, P. Davids, N. Martinez, M. Gehl, J. Chiaverini, K. Mehta, J. Romero, N. Lingaraju, A. M. Weiner, D. Peace, R. Cernansky, M. Lobino, E. Diamanti, R. Camacho, and L. Trigo Vidarte, “Roadmap on integrated quantum photonics,” J. Physics: Photonics (2021).
8. C. Chaneliere, J. Autran, R. Devine, and B. Balland, “Tantalum pentoxide (Ta2O5) thin films for advanced dielectric applications,” Mater. Sci. Eng. R: Reports **22**, 269–322 (1998).
9. S. Ezhilvalavan and T. Y. Tseng, “Preparation and properties of tantalum pentoxide (Ta2O5) thin films for ultra large scale integrated circuits (ULSIs) application – A review,” J. Mater. Sci. Mater. Electron. **10**, 9–31 (1999).
10. L. Splitthoff, M. A. Wolff, T. Grottke, and C. Schuck, “Tantalum pentoxide nanophotonic circuits for integrated quantum technology,” Opt. Express **28**, 11921 (2020).
11. M. A. Wolff, S. Vogel, L. Splitthoff, and C. Schuck, “Superconducting nanowire single-photon detectors integrated with tantalum pentoxide waveguides,” Sci. Reports **10**, 17170 (2020).
12. L. Gao, F. Lemarchand, and M. Lequime, “Exploitation of multiple incidences spectrometric measurements for thin film reverse engineering,” Opt. express **20**, 15751–15734 (2012).
13. H. H. Li, “Refractive index of silicon and germanium and its wavelength and temperature derivatives,” J. Phys. Chem. Ref. Data **9**, 658–561 (1980).
14. I. H. Malitson, “Interspecimen comparison of the refractive index of fused silica,” Josa **55**, 1209–1205 (1965).
15. J. A. Black, R. Streater, K. F. Lamee, D. R. Carlson, S.-P. Yu, and S. B. Papp, “Group-velocity-dispersion engineering of tantala integrated photonics,” Opt. Lett. **46**, 820–817 (2021).
16. P. P. J. Schrinner, J. Olthaus, D. E. Reiter, and C. Schuck, “Photophysics of single nitrogen-vacancy centers in nanodiamonds coupled to photonic crystal cavities,” arXiv preprint arXiv:2011.11111 (2020).
17. M. Belt, M. L. Davenport, J. E. Bowers, and D. J. Blumenthal, “Ultra-low-loss Ta 2 O 5-core/SiO 2-clad planar waveguides on Si substrates,” Optica **4**, 536–532 (2017).
18. A. Eich, T. C. Spiekermann, H. Gehring, L. Sommer, J. R. Bankwitz, P. P. J. Schrinner, J. A. Preuß, S. M. de Vasconcellos, R. Bratschitsch, W. H. P. Pernice, and others, “Single photon emission from individual nanophotonic-integrated colloidal quantum dots,” arXiv preprint arXiv:2104.11830 (2021).
19. Y. Zhao, M. Jenkins, P. Measor, K. Leake, S. Liu, H. Schmidt, and A. R. Hawkins, “Hollow waveguides with low intrinsic photoluminescence fabricated with Ta2O5 and SiO2 films,” Appl. Phys. Lett. **98**, 091104 (2011).
20. T. Kaji, T. Yamada, R. Ueda, X. Xu, and A. Otomo, “Fabrication of two-dimensional Ta_2O_5 photonic crystal slabs with ultra-low background emission toward highly sensitive fluorescence spectroscopy,” Opt. Express **19**, 1422 (2011).
21. M. Timmerkamp, N. M. Lüpken, S. A. Abazi, J. R. Bankwitz, C. Schuck, and C. Fallnich, “Toward integrated tantalum pentoxide optical parametric oscillators,” arXiv preprint arXiv:2306.05073 (2023).
22. K. Nisi, S. Subramanian, W. He, K. A. Ulman, H. El-Sherif, F. Sigger, M. Lassaunière, M. T. Wetherington, N. Briggs, J. Gray, A. W. Holleitner, N. Bassim, S. Y. Quek, J. A. Robinson, and U. Wurstbauer, “Light–Matter Interaction in Quantum Confined 2D Polar Metals,” Adv. Funct. Mater. **31**, 2005977 (2021).
23. H. Demiryont, J. R. Sites, and K. Geib, “Effects of oxygen content on the optical properties of tantalum oxide films deposited by ion-beam sputtering,” Appl. Opt. **24**, 490 (1985).
24. R. Ramprasad, “First principles study of oxygen vacancy defects in tantalum pentoxide,” J. Appl. Phys. **94**, 5609–5612 (2003).
25. H. Jung, S.-P. Yu, D. R. Carlson, T. E. Drake, T. C. Briles, and S. B. Papp, “Tantala Kerr nonlinear integrated photonics,” Optica **8**, 811 (2021).
26. H. Xu, M. Hafezi, J. Fan, J. M. Taylor, G. F. Strouse, and Z. Ahmed, “Ultra-sensitive chip-based photonic temperature sensor using ring resonator structures,” Opt. Express **22**, 3098 (2014).
27. H. Fujiwara, *Spectroscopic Ellipsometry* (Wiley, 2007).
28. K. Johnson, N. Alshamrani, D. Almutairi, A. Grieco, C. Horvath, J. N. Westwood-Bachman, A. McKinlay, and Y. Fainman, “Determination of the nonlinear thermo-optic coefficient of silicon nitride and oxide using an effective index method,” Opt. Express **30**, 46134 (2022).
29. J. Rodriguez, S. A. Chandorkar, G. M. Glaze, D. D. Gerrard, Y. Chen, D. B. Heinz, I. B. Flader, and T. W. Kenny, “Direct Detection of Anchor Damping in MEMS Tuning Fork Resonators,” J. Microelectromechanical Syst. **27**, 800–809 (2018).
30. K. G. Lyon, G. L. Salinger, C. A. Swenson, and G. K. White, “Linear thermal expansion measurements on silicon from 6 to 340 K,” J. Appl. Phys. **48**, 868–865 (1977).